Journal of Physical Science, Vol. 30(Supp.2), 23–40, 2019

Remarkable Catalytic Activity of CMC/$BiFeO_3$ Nanocomposite Film for the Degradation of Methyl Orange Under Direct Sunlight Radiation

Nor Atilia Athira Zaahari,[1] Teo Leong Huat,[1] Noor Haida Mohd Kaus,[1*]
Mohamad Haafiz Mohamad Kassim[2] and Muhammad Zamir Othman[3]

[1]Nano Hybrid Materials Group, School of Chemical Sciences,
Universiti Sains Malaysia, 11800 USM Pulau Pinang, Malaysia
[2]School of Industrial Technology, Universiti Sains Malaysia,
11800 USM Pulau Pinang, Malaysia
[3]Faculty of Science and Technology, Universiti Sains Islam Malaysia,
71800, Negeri Sembilan, Malaysia

[*]Corresponding author: noorhaida@usm.my

Published online: 25 December 2019

To cite this article: Zaahari, N. A. A. et al. (2019). Remarkable catalytic activity of CMC/$BiFeO_3$ nanocomposite film for the degradation of methyl orange under direct sunlight radiation. *J. Phys. Sci.*, 30(Supp. 2), 23–40, https://doi.org/10.21315/jps2019.30.s2.3

To link to this article: https://doi.org/10.21315/jps2019.30.s2.3

ABSTRACT: *Carboxymethyl cellulose (CMC)/bismuth ferrite ($BiFeO_3$) nanocomposites with optical excitation of 490 nm were successfully prepared by impregnation method and were characterised by X-ray diffraction (XRD), Fourier transform infrared (FTIR) spectroscopy, scanning electron microscope (SEM) and UV-Vis technique. The photocatalytic efficiency of the composite was further evaluated by degradation of methyl orange (MO) at wavelength 464 nm under direct sunlight irradiation. The incorporation of 0.8 w/w% $BiFeO_3$ catalyst within the CMC film had shown a remarkable removal efficiency of 10 ppm MO by 91.62% as compared to pristine $BiFeO_3$ with only 0.7% removal. There exists efficient synergistic effect of photodegradation and adsorption of MO onto CMC-$BiFeO_3$. Kinetics studies revealed that the MO removal dominantly governed by adsorption that obeys pseudo-second order kinetic model. The photocatalytic activity has high effect in acidic condition. The recycling ability of unwashed nanocomposite confirming that the photocatalyst was essentially stable.*

Keywords: Photocatalytic degradation, carboxymethyl cellulose, bismuth ferrite, methyl orange, kinetic

1. INTRODUCTION

The treatment of dye-contaminated water containing hazardous chemicals especially from the textile, printing and photographic industries is a growing need at a present time.[1] Most dyes used for dyeing and printing process are synthetic in nature and composed of aromatic ring and azo groups (N=N bond) which are highly chromatic, noxious and easily decomposed into carcinogenic aromatic amine under deoxidisation conditions when discharged into water without appropriate treatment. Methyl orange (MO) dye is one of anionic dye with azo structure that easily absorbed by skin and accumulated in the body. The presence of azo group (N=N) can cause allergies on skin contact, being toxic by inhalation and ingestion, low biodegradability and harmful to aquatic lives.[2] Therefore, the development of new materials for the removal of such dyes has been considered over the past decade.

Various efforts to treat these harmful dyes from wastewater have been dedicated in fabricating efficient adsorption materials to overcome the limitation faced by conventional adsorbents like activated carbon, zeolite and synthetic fibres.[1–3] Thus, the search for more efficient and environmental-friendly approach to combine the concept of dyes adsorption and subsequently mineralise the dyes to be environmentally compatible is essential. To date, heterogeneous photocatalysis embedded adsorbent is now considered to be a promising approach to remove organic compound efficiently from wastewater by synergising both effects.[3,4]

Bismuth ferrite ($BiFeO_3$) is a rhombohedral distorted perovskite structure of semiconductor. Owing to its superior photocatalytic abilities with high stability and narrow band gap between 2.1–2.7 eV, it is reported as one of the prominent photocatalysts under visible light or direct sunlight irradiation.[5] Despite this advantage, the separation of powdered materials from wastewater medium after the treatment becomes an obstacle and leads to the catalyst loss. Therefore, the supporting materials with adsorption properties like chitosan, cellulose, natural rubber, cellulose acetate and carboxymethyl cellulose were preferably chosen to overcome the difficulty. It is indeed behaving as an immobiliser for nanoparticles as they possess numerous advantages of good film-forming ability, biodegradability and hydrophilicity to promote the adsorption property.[6,7]

Carboxymethyl cellulose (CMC) is a water-soluble anionic polymer with derivative of carboxymethyl groups (-CH_2-COONa) bonded to several hydroxyl groups on cellulose backbone. CMC has good solubility properties, biocompatibility, non-allergenic, low toxicity and low cost. The presence of polar carboxyl groups makes the CMC soluble, chemically active, strongly hydrophilic and may increase the

interaction of water from dyes to the polymer composite.[8–12] These advantages are indeed a great importance for enabling high contact between a photocatalyst and pollutants for better effect of photodegradation.[13] Thus, this polymer has been chosen as a supporting polymer for the incorporation of $BiFeO_3$ photocatalyst with the advantages to provide good mechanical properties, high adsorption capacity and good compatibility within the system.

To the best of our knowledge, no investigation has been done on the photocatalytic activity on the removal of MO dye utilising CMC/$BiFeO_3$ nanocomposites as a model photocatalyst. Therefore, it is great opportunity to further explore the performance of CMC/$BiFeO_3$ composite film and evaluate both the adsorption ability and photocatalytic activity towards the removal of MO under direct sunlight irradiation with different parameters.

2. EXPERIMENTAL

2.1 Materials

Citric acid-1-hydrate (HmbG), carboxymethly cellulose (Sigma), methyl orange dye (QReC), hydrochloric acid, sodium hydroxide, bismuth nitrate pentahydrate (98% purity, Sigma Aldrich), iron(III) nitrate nonahydrate (98% purity, Sigma Aldrich) and carrageenan (Sigma) were used. All precursors were prepared using distilled water.

2.2 Synthesis of $BiFeO_3$ Nanoparticles

$BiFeO_3$ nanoparticles was prepared using biopolymer template method as described in literature.[4] Bismuth nitrate pentahydrate and iron(III) nonahydrate were used as precursors with ratio 2:1 and dissolved in 25 ml of distilled water. An amount of 10 ml of the mixture was mixed with 40 ml 1 wt% carrageenan and adjusted to pH 10 under constant stirring for 2 h. The obtained product was heated overnight then calcined at 550° for 2 hours to form rhombohedral $BiFeO_3$ nanoparticles.

2.3 Impregnation of $BiFeO_3$ of CMC Membrane

An amount of 1.25 g of CMC powder was dissolved in 1.04 M of citric acid solution under constant stirring. Then, different amounts of $BiFeO_3$ (0.01 g, 0.025 g, 0.05 g, 0.075 g and 0.1 g) was added to CMC paste and continued stirring for 2 h to ensure the mixture was homogeneous. The mixture was then transferred into a petri dish and dried in the oven to obtain CMC/$BiFeO_3$ nanocomposite film.

2.4 Characterisation

The crystallinity of CMC/$BiFeO_3$ film was determined by XRD analysis with a PANalytical X'Pert PRO θ–2θ equipped with graphited monochromatic CuK_α radiation (λ = 1.5406 Å) at 40 kV operation. The presence of functional groups in CMC/$BiFeO_3$ film was investigated using Perkin Elmer, Fourier transform near-infrared spectroscopy (FT-NIR) spectrometer frontier universal attenuated total reflection (ATR) sampling accessories. The scanning range used is 600–4000 cm^{-1} and resolution is 8 cm^{-1}. SEM FEI-Quanta FEG 650 was used to study surface morphology of CMC/$BiFeO_3$ nanocomposite film. The sample was coated with gold prior to characterisation.

pHzc was conducted utilising 40 ml 0.1 M $NaNO_3$ buffer solution with adjusted pH 2 to 12 with 0.1 M NaOH and 1.0 HNO_3. An amount of 0.1 g of $BiFeO_3$ in 0.5 g CMC (1:5 ratio) were added in 6 different conical flasks with above solutions and left under constant 350 rpm shaking. After 24 h, each sample were filtered and removed. Final adjusted pH solutions were recorded. A graph of pHzc against initial pH of suspension was plotted.

2.5 Photocatalytic Degradation of MO

The optimum condition of CMC/$BiFeO_3$ nanocomposite film was investigated by varying different amount of catalyst dosage on CMC film as mentioned in Section 2.3, initial concentration of MO (10 ppm, 30 ppm, 50 ppm, 70 ppm and 100 ppm) and pH of the solution (2, 4, 6, 8 and 10). The photocatalytic degradation was carried out under direct sunlight irradiation and the removal of MO was observed at wavelength 464 nm. The percentage removal efficiency of MO was calculated by using equation:

$$\text{Removal efficiency (\%)} = (1 - (C_f/C_o)) \times 100\ \% \quad (1)$$

where C_o corresponds to initial concentration of dye (ppm) and C_f corresponds to final concentration of dye (ppm).

2.6 Kinetic Study

To understand the mechanism of MO removal, the kinetic was studied by using three models: Langmuir Hinshelwood, pseudo first order and pseudo second order. The reaction was carried out under sunlight and an aliquot was collected at fixed time interval within 3 h. Through a batch of experiment, amount of removal at equilibrium, q_e (mg g^{-1}) and amount of removal at time, q_t can be determined by using the following equations:

$$q_e = \frac{(C_o - C_e)V}{m} \quad (2)$$

$$q_o = \frac{(C_o - C_t)V}{m} \quad (3)$$

where C_o corresponds to initial concentration of dye (ppm), C_e corresponds to concentration of dye at equilibrium (ppm) while C_t is concentration of dye at time t (ppm). V is the volume of dye solution in l and *m* is the mass of the catalyst or optimum or optimum catalyst in g.

2.7 Reusability of CMC/$BiFeO_3$ Nanocomposite Film

The reusability of nanocomposite film was investigated by varying the conditions of film after one cycle. The new cycle of degradation was conducted using washed catalyst and unwashed catalyst to determine the efficiency of CMC/$BiFeO_3$ film. For washed catalyst, it was placed in 50 ml of distilled water and shaken at 200 rpm for 2 h and dried at room temperature prior re-used for the next cycle, while unwashed film has been directly used after treatment.

3. RESULTS AND DISCUSSION

3.1 XRD Analysis

The X-ray diffraction (XRD) pattern of pure $BiFeO_3$, CMC and the $BiFeO_3$ embedded CMC (CMC/$BiFeO_3$) nanocomposite films were shown in Figure 1. As for the pure CMC, the diffraction peaks appeared at $2\theta = 23.32°$ and 26.07° indicating its semi crystalline phase. Meanwhile for pristine $BiFeO_3$, all peaks at 2θ values of 22.6°, 32.2°, 39.7°, 46.2°, 51.9°, 57.3° and 67.6° were indexed to (012), (110), (202), (024), (116), (300) and (220) planes, respectively. The reflections are consistent with the standard pattern of high crystallinity of rhombohedral phases of $BiFeO_3$ (JCPDS01-071-2494) and in agreement with the literature.[4,5] Among these planes, (110) plane has stronger reflection that observed in CMC/$BiFeO_3$ nanocomposite film with the existence of low intense peak at (202), (024) and (300). These results indicate the successful incorporation of $BiFeO_3$ in CMC membrane to form CMC/$BiFeO_3$ composite and the peaks become broader due to the nanosized $BiFeO_3$ crystal grows along the plane and distributed within the CMC polymer.

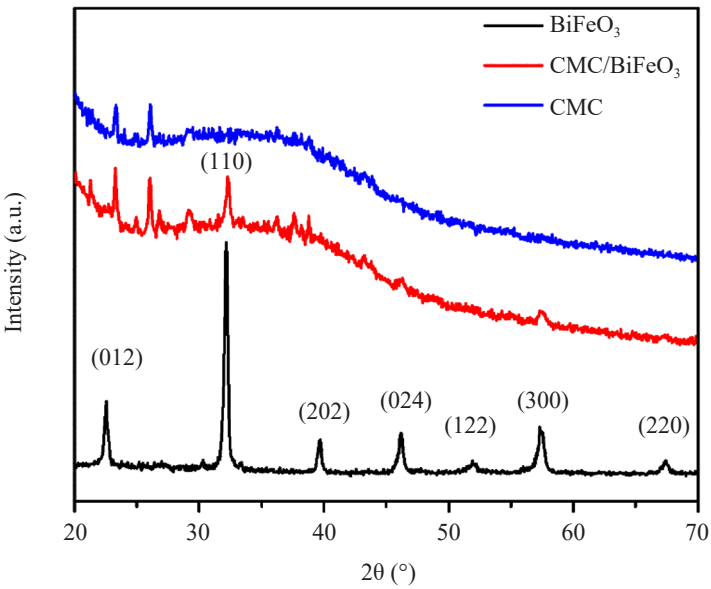

Figure 1: XRD pattern of pure $BiFeO_3$, CMC and CMC/$BiFeO_3$ nanocomposite film.

3.2 SEM

Morphology of the prepared sample were observed using secondary electron image (SEI) whereas backscattered electron image (BSEI) indicating contrasts in composition of multiphase samples. Figures 2(a and b) represent the SEI and BSEI of CMC/$BiFeO_3$ nanocomposite film, respectively, scanned at the same spot. From the SEI of CMC/$BiFeO_3$, the morphology of CMC/$BiFeO_3$ film exhibited a surface of CMC distributed with $BiFeO_3$ particles. Meanwhile at the similar spot, BSEI of the film, shown in Figure 2(b) observed the lighter part which corresponds to $BiFeO_3$ due to higher atomic number of metal whereas darker side produced from CMC polymer membrane. This result indicates that $BiFeO_3$ has successfully loaded on CMC polymer matrices. EDX analysis mapping was carried out to confirm $BiFeO_3$ particles were successful distributed in CMC membrane together with the spectrum and atomic weight composition as shown in Figures 2(c–e). The presence of C, O and Na are expected to come from the CMC membrane where the Bi and Fe are dedicated to $BiFeO_3$.

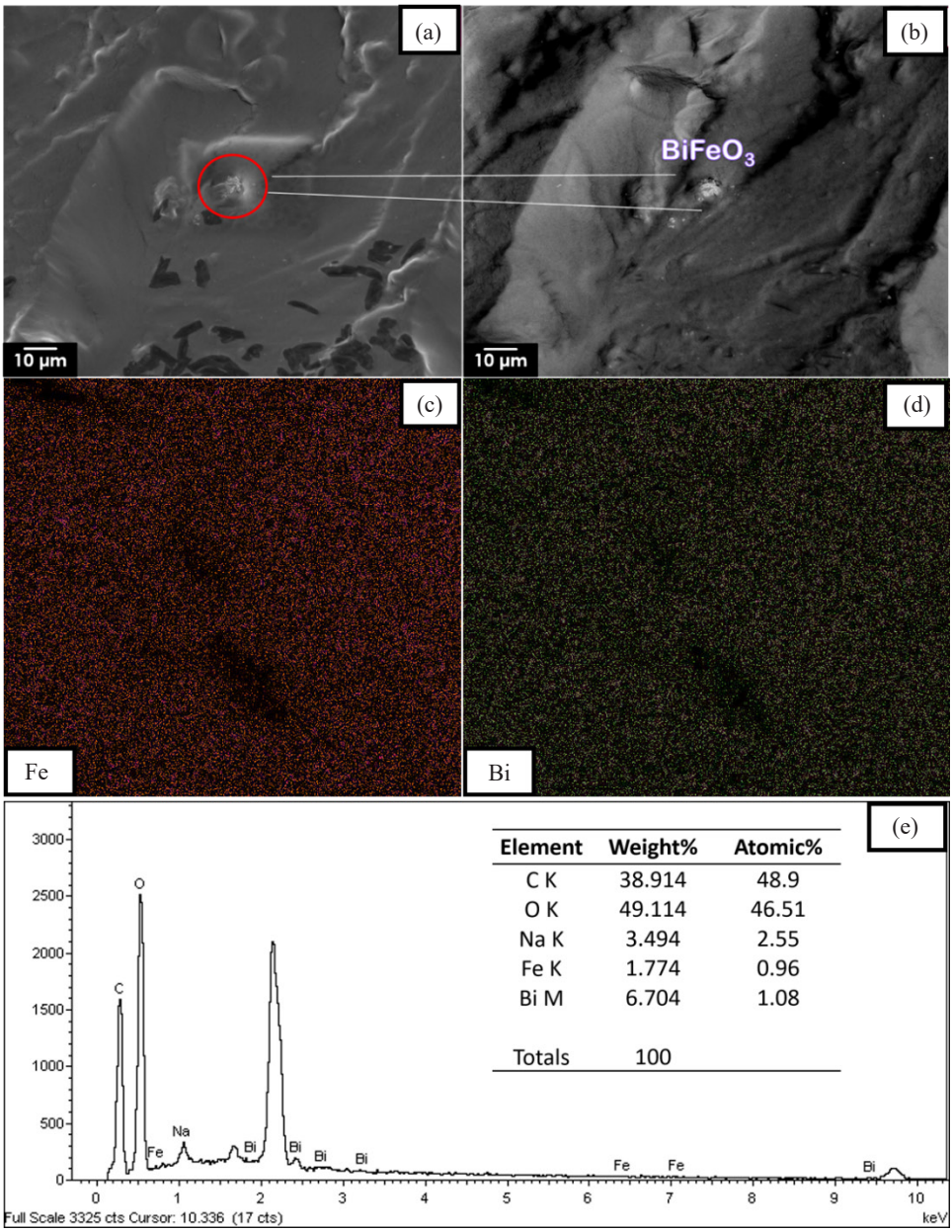

Figure 2: Morphology of (a) SEI, (b) BSEI, (c) EDX elemental mapping of Fe, (d) EDX elemental mapping of Bi, and (e) EDS spectrum of CMC/$BiFeO_3$ nanocomposite film.

3.3 FTIR

Fourier transform infrared (FTIR) spectra of pure $BiFeO_3$, CMC and CMC/$BiFeO_3$ were shown in Figures 3(a and b). The spectra of pure $BiFeO_3$ in Figure 3(a) depicts no difference from that reported in literature and the characteristic band in the -OH stretching region (3441.16 cm^{-1}) indicates the presence of symmetric of H_2O and anti-symmetric of OH^- group in $BiFeO_3$ catalyst.[4] In addition, peaks at 1636.16 cm^{-1} and 1384.36 cm^{-1} correspond to bending vibration of H_2O and trapped nitrates. Fundamental metal-oxygen bond of $BiFeO_3$ is indicated by absorption at 575 cm^{-1} which is attributed to Bi-O bond, and 442 cm^{-1} belonging to Fe-O bond was also detected.

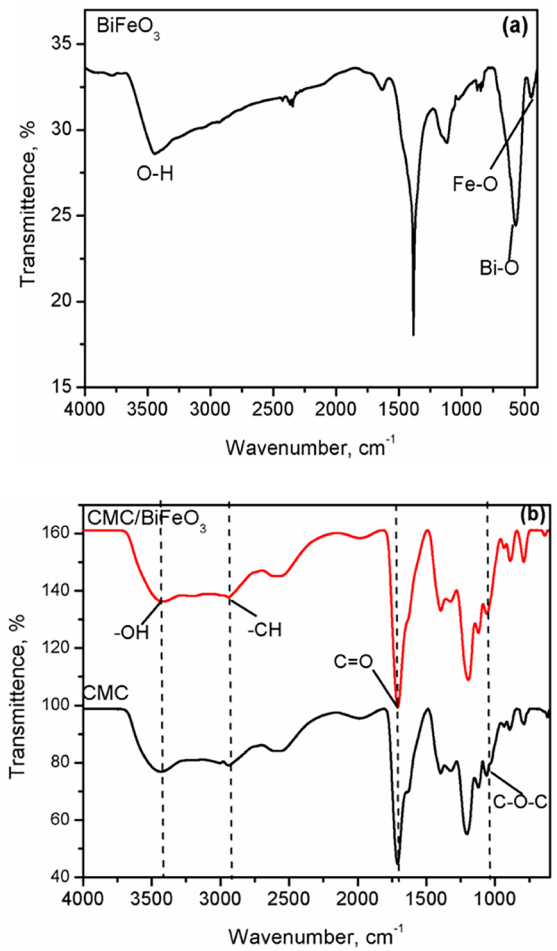

Figure 3: IR spectra of (a) $BiFeO_3$ using KBr-FTIR, and (b) CMC and CMC/$BiFeO_3$ nanocomposite films using ATR-FTIR.

Meanwhile for ATR-FTIR spectra of CMC in Figure 3(b), the peaks observed at 3428.74 cm^{-1} and 2939.16 cm^{-1} indicated the OH stretching band and CH stretching from CH_2 and CH_3 groups. Dominant adsorption peak detected at 1709.81 cm^{-1} was attributed to carboxylic group, C=O. FTIR spectrum of CMC/$BiFeO_3$ nanocomposite film showed similar absorption peaks to CMC spectrum, indicating no new bond was formed. This confirmed that only physical blending for metal distribution within the polymer matrices was involved in the process of impregnation of $BiFeO_3$ on CMC membrane. Unfortunately, the metal-oxygen bond of $BiFeO_3$ in CMC/$BiFeO_3$ film could not be detected due to limitation of instrument.

3.4 Photocatalytic Degradation of MO

In order to determine potential photocatalytic activity of the nanocomposite, the samples were conducted under direct sunlight irradiation by measuring the degradation of 50 ml of 10 ppm MO over several parameters (catalyst dosage, dye concentration, pH) within 1 h. The system was pre-conducted in dark for 60 min and then degradation proceeded at t = 0 under direct sunlight irradiation. Under dark condition, the removal efficiencies of CMC and CMC/$BiFeO_3$ nanocomposite are 25.0% and 20.0% for MO, respectively as depicted in Figure 4(a). Clearly, control CMC exhibits much higher removal ability by adsorption than the CMC/$BiFeO_3$ nanocomposite. Both samples showed rapid removal process without the presence of light at the initial stage (0–30 min) and the equilibrium is reached at 60 min. This can be attributed that MO can interact easily with the hydrophilic polymer contain the reactive sites, while slower diffusion of solute into the interior of the nanocomposites. The maximum adsorptions occur after 1 h between 20.0% to 25.0% of adsorption for both samples.

Then, various catalyst dosages of $BiFeO_3$ (0 to 100 w/w%) were introduced into the CMC matrices as shown in Figure 4(b) before investigated under direct sunlight irradiation. Control CMC film without the incorporation of $BiFeO_3$ catalyst (0 wt%) exhibited 32.3% removal under sunlight irradiation after 1 h. This can be mainly ascribed to the adsorption mechanism of the hydrophilic polymer. In case of pristine $BiFeO_3$ (100 wt%) without CMC support, the removal rate of MO is inefficient which only 0.7% removal. Interestingly, the presence of CMC/$BiFeO_3$ nanocomposite with the different $BiFeO_3$ dosage over CMC showed dominant adsorption and photocatalytic degradation towards the dye removal. The highest percentage removal of MO is found to be 91.62% for the lower dosage at 0.8(wt/wt%) of CMC/$BiFeO_3$. It is further confirmed that CMC/$BiFeO_3$ has the best photocatalytic activity not only for the removal of MO, but also to its degradation product, shown in Figure 5(c). Under direct sunlight, MO undergoes

obvious photodegradation in the presence of CMC/$BiFeO_3$ since MO shows major absorption band at 464 nm. After 180 min, the suspension was colourless, and its containing MO was degraded completely in the CMC/$BiFeO_3$-MO mixture, indicating that the dye chromophore structure was destroyed. Nevertheless, no degradation observed for MO sample treated with CMC control, shown in Figure 5(a), or pristine $BiFeO_3$, as in Figure 5(b). This indicated both samples having low adsorption towards MO removal when applied under direct sunlight.

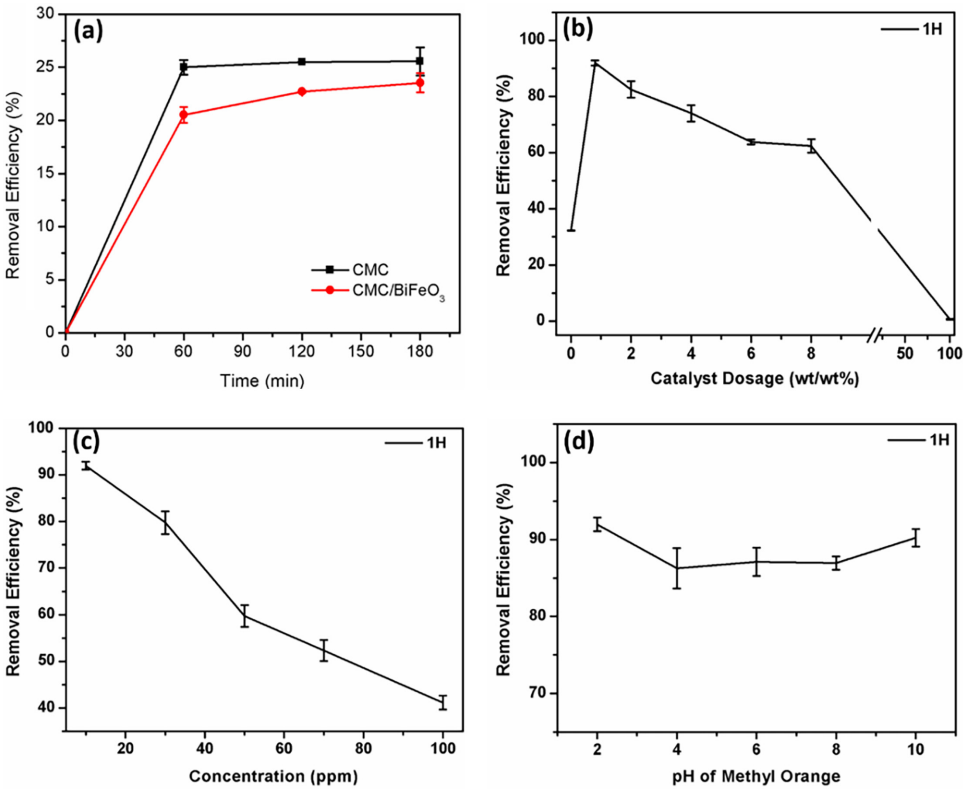

Figure 4: Removal efficiency of MO for (a) in the dark (0.8 wt% catalyst, pH 2 and 50 ml of 10 ppm MO), (b) catalyst dosage of $BiFeO_3$ on CMC membrane, (c) initial concentration of MO, and (d) pH of MO. Conditions: 50 ml of 10 ppm MO, 1 h, pH 2.

As the amount of $BiFeO_3$ increased from 0.8 wt% to 8 wt%, the percentage removal of methyl orange decreased within 1 h. Initially, the optimum quantity of catalyst would produce more OH and O_2 radicals, therefore the number of active sites on surface catalyst increased and the degradation rate rose. However, when the concentration of catalyst exceeded the optimum value, the degradation rate decreased due to difficulty in mass transfer within the system. Furthermore, increment in catalyst dosage that render the mass transfer will cause high number of unsaturated sites of the composite available in the system. This will subsequently prevent the pollutant to reach the active site of $BiFeO_3$ within the polymer support.[11] As a result, the number of OH radical decreased, hence the efficiency of degradation reduced accordingly.

With optimum catalyst loading 0.8 (wt/wt%) on the composite, the effect of different initial concentration of MO which range from 10 ppm to 100 ppm under direct sunlight irradiation was studied and depicted in Figure 4(b). The result elucidates that the percentage of MO removal gradually decreased from 91.62% to 62.77% as the dye concentration increased from 10 ppm to 100 ppm, respectively within 1 h. The removal efficiencies decreased when higher concentration of dye used within 60 min and this might be due to reduction of path length of photon to reach the catalyst surface. Therefore, longer time is required to remove higher concentration of MO efficiently.

Figure 4(c) illustrates the photocatalytic removal of dye when a series of pH level of MO were studied. As depicted from the plot, CMC/$BiFeO_3$ nanocomposite film worked efficiently in pH 2 with the degradation of 91.96%. The variation of pH changed the surface charge of composite and shifted the potentials of catalytic reactions. MO has high effect of photodegradation by the presence of CMC/$BiFeO_3$ nanocomposite in acidic condition. pH variation of solution can influence the interaction of dye molecules onto the nanocomposite surface due to different surface charge attained on it at different pH. Therefore, the experiment of point of zero charge (PZC) was carried out and it is found that pH at PZC, pH_{PZC} is 2.24 (Figure 6). At this condition, possible explanation for better removal of MO is due to the favourable pH for adsorption and the degradation of charged pollutants (pKa = 3.4). The reduction on the removal above pH 2 might be due to the deprotonated of MO, hence reducing the electrostatic interaction between positive charge in low pH and negative charge from the deprotonated ion of MO. At higher pH of methyl orange, the removal rate shows positive effect which may be due to the presence of photocatalytic intermediate that was able to degrade at higher pH level.

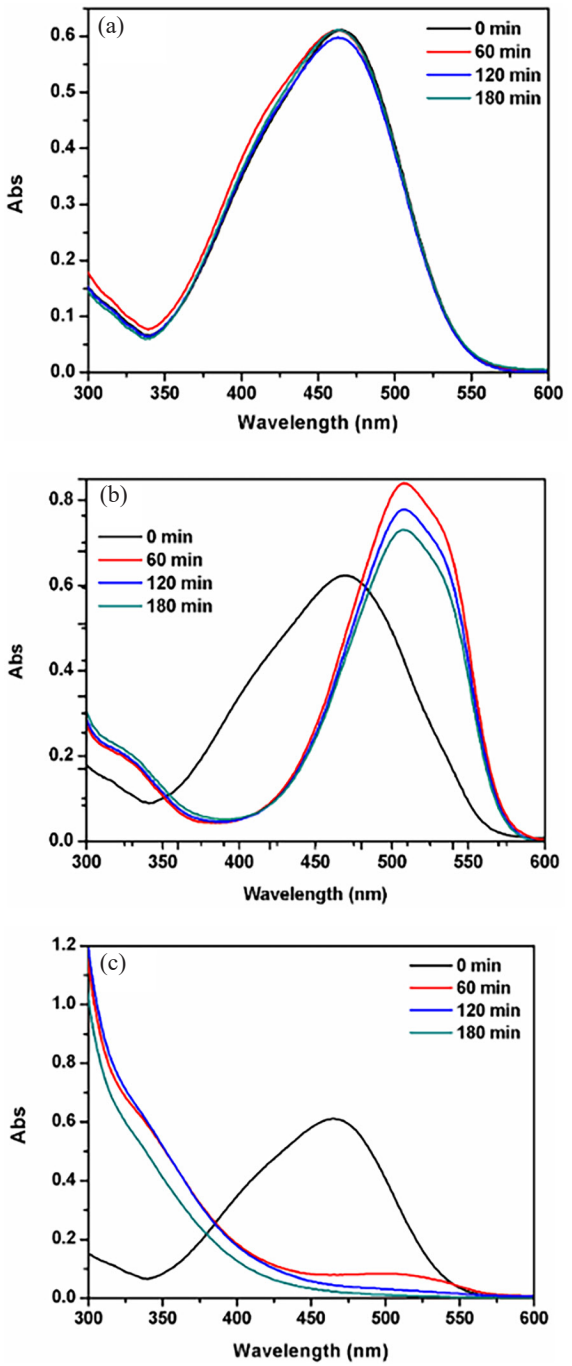

Figure 5: Absorbance of MO after being treated with (a) $BiFeO_3$ powder, (b) CMC, and (c) CMC/$BiFeO_3$ for 180 min under direct sunlight.

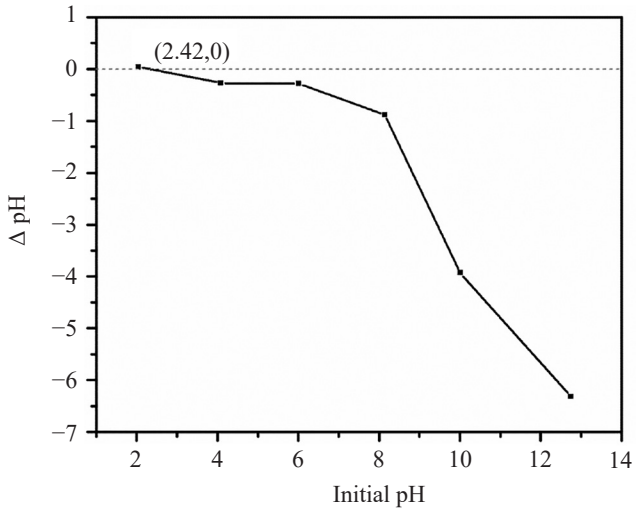

Figure 6: Plot of pH_{PZC} of CMC/$BiFeO_3$ nanocomposite.

3.5 Kinetic Study

The rate constant and kinetics order reaction were studied using kinetics models of Langmuir Hinshelwood, pseudo first order, and pseudo second order. Each of the models' graph were shown in the following Figure 7. The calculated parameters from Langmuir Hinshelwood, pseudo first order and pseudo second order models were summarised in Table 1.

Table 1: The calculated parameter for Langmuir Hinselwood, pseudo first and second order kinetic models with correlation coefficients (R^2).

Langmuir Hinshelwood			Pseudo first order			Pseudo second order		
q_e (mg g^{-1})	k_{LH} (min^{-1})	R^2	q_e (mg g^{-1})	k_1 (min^{-1})	R^2	q_e (mg g^{-1})	k_2 (min^{-1})	R^2
65.0044	0.0102	0.7895	21.1092	0.0166	0.6277	65.3595	2.0663×1^{-5}	0.9970

Based on Langmuir Hinselwood plot, the value of rate constant was obtained from the slope since its equation of kinetic model is expressed as in Equation 4:

$$\ln C_o/C_t = kt \quad (4)$$

The value of rate constant, k_{LH} and correlation coefficients (R^2) of Langmuir Hinselwood are found to be 0.0102 min^{-1} and 0.7895, respectively. While, pseudo first order, pseudo second order models were used to obtain the value calculated of q_e through the straight-line equation of kinetic reaction as following:

$$\ln(q_e - q_t) = \ln(q_e) - k_1 t \quad (5)$$

$$t/q_t = t/q_e + 1/k_2 q_e^2 \quad (6)$$

According to the pseudo first order model, the values of rate constant and q_e were calculated from the slope and intercept from the plots. The experimental values did not fit with the calculated values, which means the first-order model does not represent the adsorption kinetic of MO on the CMC/$BiFeO_3$.

In contrast, the calculated values of using pseudo second order model fitted well with the experimental data. Therefore, this model is more likely to predict the behaviour over the whole experimental range of MO adsorption more than pseudo-first-order model. Furthermore, the R^2 of 0.997 validated that adsorption and photodegradation of MO dye obeys pseudo second order kinetics. The results revealed that higher rate constant, $k = 2.0663 \times 10^{-5}$ min^{-1} were obtained using nanocomposite for the degradation of MO dye under sunlight irradiation. In this model, the surface adsorption that involves chemisorption, where the removal from solution is due to the physicochemical interactions between two phases.[12]

From the results, the incorporation of $BiFeO_3$ nanoparticles into CMC polymer resulted in a notable improvement in photocatalytic performance towards MO, in comparison to the photocatalytic performance of the non-composite materials. The enhancement can be attributed from several possible factors. The presence of CMC in the system shows enhancement of adsorption and further synergises with photodegradation effect resulted from the close contact of hydrophilic surface of catalyst and the pollutants. Meanwhile, the small size in nanometre level of $BiFeO_3$ crystal particles can benefit the catalyst to exhibit better photocatalytic activity.

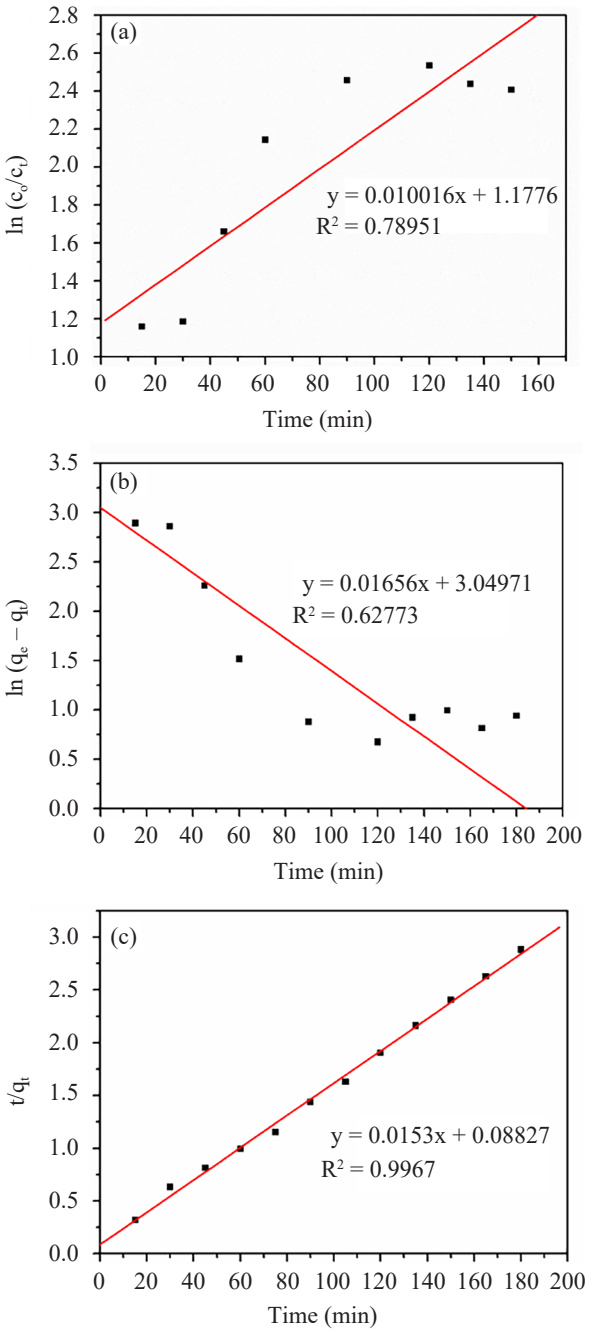

Figure 7: The linear fitting plots of the (a) Langmuir-Hinshelwood, (b) pseudo first order, and (c) pseudo second order kinetic models of 10 ppm MO removal by CMC/ $BiFeO_3$ nanocomposite.

3.6 Reusability of CMC/$BiFeO_3$ Nanocomposite Film

Reusability of catalyst is a key feature for analysing their potential applicability for industrial applications and wastewater remediation. Figure 8 exhibits the percentage of removal for four cycles after 1 h under the irradiation. The unwashed CMC/$BiFeO_3$ film showed better removal efficiency compared with the washed CMC/$BiFeO_3$ composite after reusing at least up to five cycles. However, after four consecutive runs, the activity of degradation from both films decreased rapidly and it was likely due to leaching of catalyst from composite film. It can be noted that, further enhancement on the mechanical properties of the film should be investigated for better reusability.

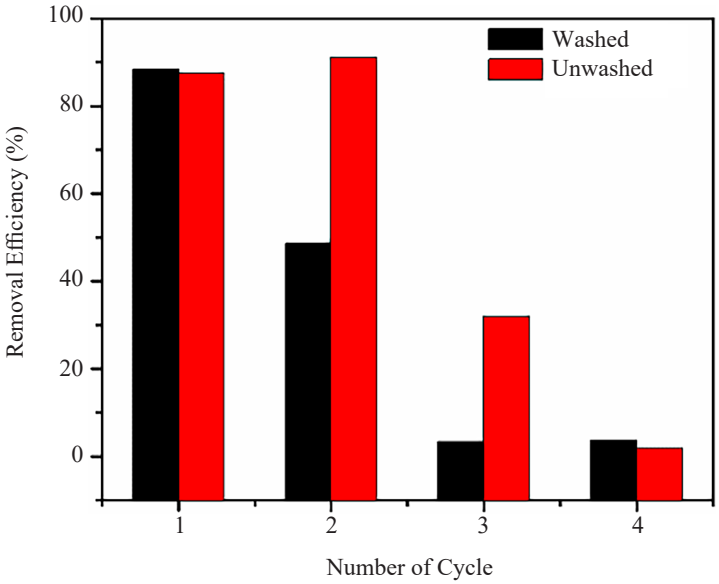

Figure 8: Reusability of CMC/$BiFeO_3$ nanocomposite film in two conditions, i.e., washed and unwashed after one cycle.

4. CONCLUSION

The $BiFeO_3$ incorporated CMC as photocatalyst composite had been successfully synthesised via facile impregnation method and its efficiency on the degradation of MO were investigated. The study significantly found that the degradation of MO was remarkably improved compared with pristine $BiFeO_3$, which has low adsorption capacity on MO. Degradation of MO dye was influenced by various parameters such as initial dye concentration, pH and catalyst dosage. Among all the investigated samples, it is found that 0.8 wt/wt% of $BiFeO_3$ on CMC film exhibited

highest photodegradation efficiency with fast and best efficient removal of MO. The dye is almost completely photodegraded when applied under the composite system. The system also shows positive effect towards the degradation of various initial concentration of MO at optimum condition. The kinetic studies revealed that MO degradation process obey pseudo second order kinetic model. Moreover, the experiment showed that unwashed composite showed better removal efficiency than washed composite and can be recyclable up to four consecutive cycles. Besides, the composite had the potential to be utilised as an efficient photocatalyst, to remove various organic dyes and pollutants under naturally available sunlight.

5. ACKNOWLEDGEMENTS

This research was financially supported by Research University (RUI) grant 1001/PKIMIA/8011069 and 203/PKIMIA/6711792 allocated by Universiti Sains Malaysia and Ministry of Higher Education Malaysia.

6. REFERENCES

1. Alqaragully, M. B. (2014). Removal of textile dyes (maxilon blue, and methyl orange) by date stones activated carbon. *Int. J. Adv. Res. Chem. Sci.*, 1(1), 48–59.
2. Ghaly, A. E. et al. (2014). Production, characterization and treatment of textile effluents: A critical review. *J. Chem. Eng. Process Technol.*, 5(1), 1–18, https://doi.org/10.4172/2157-7048.1000182.
3. Chaturvedi, S. & Pragnesh, N. D. (2015). Environmental application of photocatalysis. *Mater. Sci. Forum*, 734, 273–294, https://doi.org/ 10.4028/www.scientific.net/MSF.734.273.
4. Azmy, H. A. et al. (2017). Visible light photocatalytic activity of $BiFeO_3$ nanoparticles for degradation of methylene blue. *J. Phys. Sci.*, 28(2), 85–103, https://doi.org/10.21315/jps2017.28.2.6.
5. Satar, N. S. A. & Kaus, N. H. M. (2016). Experimental and first-principles investigations of lattice strain effect on electronic and optical properties of biotemplated $BiFeO_3$ nanoparticles. *J. Phys. Chem. C*, 120, 26012–26020, https://doi.org/10.1021/acs.jpcc.6b08548.
6. Zhao, X. et al. (2011). Polymer-supported nanocomposites for environmental application: A review. *Chem. Eng. J.*, 170, 381–394, https://doi.org/10.1016/j.cej.2011.02.071.
7. Singh, S., Mahalingam, H. & Singh, P. K. (2013). Polymer-supported titanium dioxide photocatalysts for environmental remediation: A review. *Appl. Catal. A Gen.*, 462–463, 178–195, https://doi.org//10.1016/j.apcata.2013.04.039.
8. Zheng, W. J. et al. (2015). Facile fabrication of self-healing carboxymethyl cellulose hydrogels. *Eur. Polym. J.*, 72, 514–522, https://doi.org/10.1016/j.eurpolymj.2015.06.013.

9. Demitri, C. et al. (2008). Novel superabsorbent cellulose-based hydrogels crosslinked with citric acid. *J. Appl. Phys. Sci.*, 110, 2453–2460.
10. Reeves, R. et al. (2010). Synthesis and characterization of carboxymethylcellulose-methacrylate hydrogel cell scaffolds. *Polym.*, 2, 252–264, https://doi.org/10.3390/polym2030252.
11. Petit, M. et al. (2016). An introduction to photocatalysis through methylene blue photodegradation. *Eur. J. Phys.*, 37(6), 065808, https://doi.org/10.1088/0143-0807/37/6/065808.
12. Robati, D. (2013). Pseudo-second-order kinetic equations for modeling adsorption systems for removal of lead ions using multi-walled carbon nanotube. *J. Nanostr. Chem.*, 3, 3–8, https://doi.org/10.1186/2193-8865-3-55.
13. Araujo, P. Z. et al. (2010). Aerosol assisted production of mesoporous titania microspheres with enhanced photocatalytic activity: The basis of an improved process. *ACS Appl. Mater. Interf.*, 2, 1663–1673, https://doi.org/10.1021/am100188q.